Cleaner Engineering and Technology 6 (2022) 100398

Contents lists available at ScienceDirect

Cleaner Engineering and Technology

journal homepage: www.sciencedirect.com/journal/cleaner-engineering-and-technology

Alkali-activated fly ash-blast furnace slag blend rheology: Evaluation of yield and Maxwell responses

Kondepudi Kala, Kolluru V.L. Subramaniam *

Department of Civil Engineering, I.I.T. Hyderabad, Hyderabad, Telangana, India

ARTICLE INFO

Keywords:
Yield stress
Maxwell flow
Thixotropy
Fly ash-slag blend
Alkali-activated

ABSTRACT

The rheological behavior of pastes made with fly ash-slag blends in alkali silicate activating solutions is evaluated. The link between the activating solution composition and the fundamental rheological behavior of alkali-activated pastes are studied for different fly ash-slag blends. The transient response of alkali-activated pastes prior to initiation of flow under an applied strain rate varies between yield-type or Maxwell-flow behaviors depending on the silica content in the activating solution. Adding dissolved silica in the alkaline activating solution initially produces a decrease in the yield stress of the paste, but with further increase the transient response transitions to a Maxwell-flow type behavior. Maxwell flow behavior is a fluid-dominated response with an apparent yield stress in the transient response under constant applied strain rate. The apparent yield stress in the Maxwell flow response increases sensitively with increasing silica content in the activating solution. On increasing the silica content in the activating solution, there is an increase in the plastic viscosity of the pastes. The thixotropy of the paste is influenced by the silica content in the activating solution and the slag content in the blend. Blends with yield-type behavior exhibit a rapid yield stress recovery after shearing. The yield stress and the structural rebuilding energy (SRE) increase very rapidly with age in activated mixtures containing dissolved silica. The pastes which exhibit Maxwell flow response have a significantly slower structural buildup indicated by a lower rate of increase in the SRE with age compared to material with yield type of behavior. The slag content in the blend contributes to a rapid increase in the SRE. The requirements of rheology control of the paste for different processing requirements including pumping and 3D concrete printing are evaluated.

1. Introduction

Concrete made with a cementitious binder is the most prevalently used construction material. The production of cement accounts for 8% of anthropogenic CO_2 emissions, which is related to the energy of processing and the decomposition of the source materials (Makul 2020). Geopolymers are considered as environmentally friendly and sustainable construction materials. Geopolymers are synthesized from variety of waste materials reducing the impact on environment (Benito et al., 2013). Replacing ordinary Portland cement with supplementary cementitious materials has conventionally been tried to reduce the carbon footprint of cement (Yang et al., 2015). The production of concrete with geopolymers and alkali-activated binders is now being explored as a sustainable alternative to cement. These binders typically use post-industrial waste materials and have lower environmental and energetic impacts while providing adequate mechanical properties for most construction applications. These binders allow for more efficient utilization of post-industrial waste materials in much larger quantities than is possible in conventional concrete mixtures. The durability of the alkali-activated binders depends on the microstructure of the products formed in the system (Bernal and Provis 2014). It can be controlled by the adjusting the fly ash/slag binder ratios, dosage of activators and admixtures (Arbi et al., 2016). The chloride penetration rates are less in alkali binders compared to Portland cement and these binders are highly resistant to fire and freeze-thaw cycles (Pacheco-Torgal et al., 2012). The compact structure of alkali-activated binders resists the water penetration into the surface of the concrete (Fu et al., 2011). The addition of fly ash increases the sulphate resistance of the concrete (Yaragal et al., 2020). Alkali-activated binders suffer less deterioration compared to Portland cement when exposed to sulphuric acid (Albitar et al., 2017).

Geopolymers are typically produced by alkali-activation of a low-calcium fly ash binder. Typically, sodium-based alkaline activators containing dissolved silica are used. The most commonly used activating

* Corresponding author.
E-mail addresses: ce17resch01006@iith.ac.in (K. Kala), KVLS@ce.iith.ac.in (K.V.L. Subramaniam).

https://doi.org/10.1016/j.clet.2022.100398
Received 15 March 2021; Received in revised form 13 December 2021; Accepted 31 December 2021
Available online 5 January 2022
2666-7908/© 2022 The Authors. Published by Elsevier Ltd. This is an open access article under the CC BY-NC-ND license (http://creativecommons.org/licenses/by-nc-nd/4.0/).

solutions are combinations of sodium hydroxide (NaOH) and sodium silicate ($Na_2O.xSiO_2$). An alkali-activated fly ash paste (AAF) is a particulate suspension of the fly ash in a viscous alkali silicate solution. Exposure to the alkaline solution leads to the dissolution of the glassy phase in the fly ash and the release of precursors for geopolymer production. The activating solution supplements the requirement of sodium and silica in the geopolymer (Duxson et al., 2007). The formation of gel in the alkali-activated binders depends on the Si/Al ratios (Zhuang et al., 2016). However, the addition of sodium silicate produces a higher viscosity (Zannerni et al., 2020). The exact requirements of sodium, dissolved silica, and NaOH molarity in the activating solution for producing high strength geopolymers from low-calcium fly ash with given reactive silica and alumina contents depend on the reactive content of the fly ash (Bhagath Singh and Subramaniam 2017). The compressive strength depends on the content of the amorphous reaction content formed (Bhagath Singh and Subramaniam 2019a). The compressive strength is reported to directly proportional to the Si: Al atomic ratio in the product (Bhagath Singh and Subramaniam 2020). Producing geopolymers from alkali activation of low-calcium fly-ash, however, needs heat curing for early strength properties (Chithiraputhiran and Neithalath, 2013). The increase in the silica content relative to alumina is not influenced by solution molarity or temperature (Bhagath Singh and Subramaniam, 2017). The addition of a calcium source, such as GGBS to the fly-ash reduces the setting time and produces strength gain under ambient conditions (Ravikumar et al., 2010). The addition of slag affected the reaction product and the silica structure (Lee and Lee, 2015). The increased additions of slag increase the C–S–H gel formation and decrease the aluminosilicate gel (Ye and Radlińska, 2016). Utilization of coal ash based byproducts in alkali cements improved the rheological and compressive properties (Samarakoon et al., 2019).

AAF pastes are shear thinning (or pseudoplastic) with increasing strain rates (Lootens et al., 2004). The shear thinning of the materials can be related to the decrease in size of the structure with the increasing shear rate (Vázquez-Quesada et al., 2016). The zeta potential between the particles is the index of particle aggregation capacity (Kondepudi and Subramaniam 2019). The paste rheology depends on the viscosity of the activating solution. The AAF pastes exhibited higher viscosity and lower yield stress properties compared to Portland cement. The thixotropy exhibited by the AAF pastes depends less on the fly ash itself and is determined by the composition of the activating solution. The thixotropy in fly ash based geopolymers with higher silica dosages is low (Kondepudi and Subramaniam 2019). The alkali silica-based fly ash geopolymers exhibit rate dependent behavior due to high viscous nature (Gadkar and Subramaniam 2019). Alkali-activated slag (AAS) pastes exhibit complex rheological behavior, which depends on the alkali modulus (M_S), which is the mass ratio of SiO_2 to Na_2O in the activating solution (Palacio et al., 2008). The fundamental rheological behavior inferred from model fits to viscometric measurements indicates a yield-type behavior, which increases with Na_2O content in the activating solution (Palacio et al., 2008). The addition of silica to slag in an alkaline solution has been shown to decrease the yield stress in sodium silicate activated slag suspensions (Puertas et al., 2014). AAS is shown to be rapidly aging with increasing alkalinity resulting in a fast evolution of rheological properties with time (Palacio et al., 2008). The addition of silica in the alkali activated slag decreases the Ca/Si ratio in the system, producing reaction products with higher mechanical strength and lower porosity (Puertas et al., 2014). The loss in the workability of slag in alkaline solution is also accelerated with the addition of soluble silica (Chang 2003). AAS with silica contents exhibits faster setting times due to early product formation (Fernández-Jiménez and Puertas, 2001); The sodium in the presence of the silica in slag-based system leads to accelerating effect in the calcium silicate hydrate product formation (Reddy et al., 2020).

Binders made with fly ash-slag blends are being actively developed to overcome the slow strength gain when only fly ash is used and the rapid uncontrolled setting in alkali-activated slags. Alkali-activated blends of slag and fly ash (AAFS) have better control over setting behavior when compared to AAS and achieve strength gain at room temperature curing unlike AAF (Lee and Lee, 2013). Fly ash in the binder improves the workability of the alkali-activated blend. The improvement is related to a decrease in the viscosity and yield stress (Yang et al., 2018). While slag in the binder results in reduced flowability of the alkali-activated blend, it allows a room temperature curing (Fang et al., 2018). There is a reduction in the workability of fly ash slag blends in activating solutions containing dissolved silica (Gao et al., 2015).

The studies in the literature are confined mostly to the mechanical properties, setting behavior, and microstructure of the AAFS. The setting time is highly dependent on the activator concentration (Marjanović et al., 2015). The desirable workability and setting time can be attained by blending fly ash with the slag (Nath and Sarker 2014). Longer mixing times decreases the thixotropy in AAS systems (Puertas et al., 2018). The additions of nano silica aids in speeding up the hydration of material. (Lavergne et al., 2019). Replacing natural sand with copper slag at appropriate levels increased the fluidity and mechanical strength (You et al., 2020). Developing applications like self-leveling concrete, 3D concrete printing, and cellular concrete using the AAFS requires understanding their rheological behavior (Alghamdi et al., 2019). Rheological characterization of these complex binder systems considering the influences of the blend composition, solids loading, and activating solution composition is required.

In this paper, AAFS pastes made using sodium-based alkaline activating solutions with dissolved silica are evaluated. In these activated binders, external silica is required in the activating solution for achieving adequate strength after hardening (Bhagath Singh and Subramaniam, 2017). Additionally, an adequate concentration of [OH^-] is required in the activating solution to ensure the reactivity of fly ash (Bhagath Singh, and Subramaniam, 2019b). This research extends the knowledge on the influences of mass proportions of source materials and activating solution compositions on the rheological properties of AAFS binder. An understanding on the effect of silica content and the alkalinity in the activating solution on the onset of flow behavior along with the structural rebuilding energy of the AAFS is determined.

2. Materials and methods

2.1. Source materials

The source materials consisted of low-calcium siliceous fly ash and ground granulated blast furnace steel slag (hereafter referred to as slag). The particle size distributions of these materials are shown in Fig. 1. The

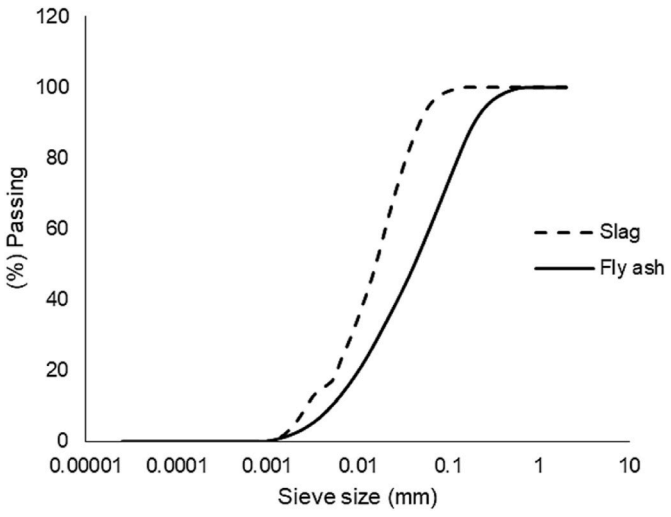

Fig. 1. Size distributions of slag and low-calcium fly ash used as source materials.

median particle sizes of the fly ash and slag were 43.1 μm and 15.8 μm, respectively. The oxide compositions of fly ash and slag are listed in Table 1. The proportions of reactive SiO_2 and Al_2O_3 contents in the fly ash were equal to 27.1% and 16.0%, respectively, while the total SiO_2 and Al_2O_3 contents were 55.7 and 26.0%, respectively. The Rietveld-based quantitative analysis was performed to identify the phases in the material using the TOPAS software. The known crystalline structures were extracted based on the Inorganic Crystal Structure Database (ICSD), and the glassy phase was separated using hkl phase structural factors. The phase quantification of individual compounds was performed using the external standard method based on the Rietveld scale factors (Bhagath Singh et al., 2018). The reactive forms of SiO_2 and Al_2O_3 are available in a glassy phase, and the difference between the total and reactive SiO_2 and Al_2O_3 is present in non-reactive, crystalline forms. The fly ash and slag conformed to IS 3812–2013 and IS 12089–1987 respectively for use as pozzolans in concrete. Class F fly ash requirements of ASTM C618 were also satisfied.

2.2. Activating solution

The alkali-silicate pastes were made by mixing the activating solutions with blends of fly ash and slag. The activating solutions were combinations of sodium hydroxide (NaOH) and sodium silicate ($Na_2O.xSiO_2$). A commercially available $Na_2O.xSiO_2$ solution with mass proportions of Na_2O: SiO_2: H_2O equal to 14.7: 34.2: 51.1 was used. The pH of the $Na_2O.xSiO_2$ solution was 13.47.

2.3. Binder compositions

AAFS binder pastes were made with blends with different mass proportions of fly ash and slag. Three series of blends with mass proportions of fly ash to slag equal to 50:50, 80:20, and 90:10 designated as F50S50, and F80S20, and F90S10, respectively, were considered in the experimental program. Additionally, alkali-silicate activated fly ash designated F100S0 was also considered for reference. In the experimental program, the activating solution composition was varied for each blend proportion. For each series of blends, alkali-activated solutions were prepared with varying silica content (mass proportion of SiO_2/H_2O in the solution) while keeping the molarity of NaOH in the activating solution equal to 3 M. The molarity of NaOH reported in this study refers to the final molarity of NaOH in the activating solution. This was calculated as the number of moles of NaOH per liter of water in the final solution. It may be noted that the final molarity of NaOH is used in this study as opposed to the initial molarity of NaOH used to prepare the solution as reported in previous studies. The final molarity, therefore, provides an indication of the $[OH^-]$ in the solution. The rheological properties of the suspension are controlled by the final concentrations in the activating solution considering all the ingredients. The NaOH concentration, which provides an $[OH^-]$ of 3 M in the activating solution was adequate for achieving the highest strength gain in the alkali-activated fly ash and slag (Bhagath Singh, G.V., and Subramaniam, 2017). The practical use of materials in site is possible through considering low to medium molarity (Reddy et al., 2020).

Table 1
Mass percentages of oxides in the fly ash and slag.

Oxide	Fly-ash	Slag
SiO_2	55.7	29.7
Al_2O_3	26.0	16.4
CaO	4.1	43.1
Fe_2O_3	5.6	0.9
MgO	1.9	4.7
K_2O	2.8	0.8
TiO_2	1.8	1.1
SO_3	0.9	2.2
P_2O_5	0.6	–
MnO	0.7	–
Loss on ignition (%)	0.09	1.50

The rheology of the activating solution, which is prepared by mixing NaOH with $Na_2O.xSiO_2$, is determined by two factors, the silica content, and the M_S (Kondepudi and Subramaniam, 2019). The static viscosity increases with the increase in modulus when it becomes either siliceous or alkaline (Yang et al., 2008). There is an increase in the M_S of the activating solution with an addition of dissolved silica. The M_S of all the activating solution were smaller than 1.80, which ensured a colloidal form of silica in the solution (Kondepudi and Subramaniam, 2021a). The viscoelastic measurements aids in understanding material behavior below elastic limit (Saak et al., 2001). The alkali-silicate activating solution is known to behave as a Newtonian fluid (Kondepudi, K., and Subramaniam., 2019). The increase in the silica content produces an increase in the viscosity of the activating solution. Further, in the range of $M_S < 1.80$, at a constant silica content, increasing the M_S in the activating solution produces a decrease in its viscosity (Kondepudi and Subramaniam, 2019). The viscosity of the activating solution provides a basis for interpreting the changes in the rheological behavior of the AAFS pastes with the activating solution composition. The rheological results depend on the type of geometry used. The vane geometry is known to produce a cylindrical shearing surface defined as diameter and height (Olivas et al., 2016).

2.4. Solids loading and mix designations

The alkali-activated pastes were prepared with different solids loadings given by the different mass proportions of the activating solution to source materials in the blend (*sol/b*) equal to 0.385, and 0.42. The test matrix along with mix designations of all the pastes considered in the experimental program are listed in Table 2. The AAFS pastes are identified with the notation FAASBB-XX-YY, where AA, and BB, refer to the mass proportions of fly ash and slag in a series, XX refers to the *sol/b* ratio in the paste and YY refers to the silica content in the activating solution. In the experimental test matrix, the influence of the solids loading is indicated by the *sol/b* ratio, the composition of the blend is indicated by the FAASBB, and the composition of the activating solution is indicated by the silica content. The M_S of the activating solution is also listed in Table 2. All the blends in the series containing slag exhibited setting under ambient conditions of 27 deg C. The initial setting times of four mixtures, F50S50-0.42–0, F50S50-0.42–0.33, F90S10-0.42–0, and F90S10-0.42–0.33, which cover the ranges of slag and silica contents were determined from Vicat penetration measurements and were 2 h, 1 h 15 min, 4 h 45 min, and 6 h, respectively.

2.5. Mixing and pre-shear protocols

The alkali-activated pastes conforming to the mass proportions listed in Table 2 were prepared by mixing the blends of fly ash and slag with the activating solutions at 300 rpm for 150 s. The alkali-activated paste was placed in the cup of the rheometer and pre-shared at 20 s^{-1} for 120 s using the vane. The paste samples were then allowed to equilibrate for 120 s before starting the rheological measurements. The same pre-shearing procedure was followed for all the mixtures to maintain an identical shear history prior to testing.

3. Rheological measurements

The experimental test procedures for determining the yield stress, viscosity, and thixotropy of the alkali-activated pastes were developed and are described in detail in (Kondepudi, K., and Samarakoon et al., 2019). A brief review is presented here for completeness. The rheological measurements were performed using the cup and vane system in a strain-controlled rheometer. The setup consisted of a concentric four-bladed vane of 28 mm diameter in a 30 mm diameter cup. The cup and vane measurement system were used to avoid potential inaccuracies

Table 2
The test matrix showing the different blend proportions, solids loading, and activating solutions compositions.

Series	Sol/b	Activating solution		Designation	Yield stress (Pa)	Apparent viscosity (Pa.s)	Plastic viscosity (Pa.s)
		SiO_2/H_2O	M_S				
F50S50	0.385	0	0	F50S50-0.385-0	23.0	–	1.0
		0.09	0.67	F50S50-0.385–0.09	22.0	–	2.7
		0.18	1.03	F50S50-0.385–0.18	–	15.0	8.9
		0.27	1.27	F50S50-0.385–0.27	–	64.0	40.2
	0.42	0	0	F50S50-0.42-0	15.6	–	0.5
		0.09	0.66	F50S50-0.42–0.09	6.8	–	1.1
		0.23	1.18	F50S50-0.42–0.23	–	15.5	9.7
		0.33	1.38	F50S50-0.42–0.33	–	54.3	36
F80S20	0.385	0	0	F80S20-0.385-0	10.0	–	0.4
		0.09	0.67	F80S20-0.385–0.09	5.5	–	0.8
		0.18	1.03	F80S20-0.385–0.18	–	5.2	2.7
		0.27	1.27	F80S20-0.385–0.27	–	12.5	8.7
	0.42	0	0	F80S20-0.385-0	6.9	–	0.3
		0.09	0.66	F80S20-0.385–0.09	2.2	–	0.4
		0.23	1.18	F80S20-0.385–0.23	–	4.7	2.6
		0.33	1.38	F80S20-0.385–0.33	–	15	9.8
F90S10	0.385	0	0	F90S10-0.385-0	7.9	–	0.3
		0.09	0.67	F90S10-0.385–0.09	3.0	–	0.6
		0.18	1.03	F90S10-0.385–0.18	–	3.1	1.8
		0.27	1.27	F90S10-0.385–0.27	–	9.0	7.5
	0.42	0	0	F90S10-0.42-0	5.0	–	0.2
		0.09	0.66	F90S10-0.42–0.09	1.70	–	0.3
		0.23	1.18	F90S10-0.42–0.23	–	3.2	1.2
		0.33	1.38	F90S10-0.42–0.33	–	14.0	8.6
F100S0	0.42	0	1.27	F100S0-0.42-0	3.1	–	0.1
		0.09	0	F100S0-0.42–0.09	1.0	–	0.3
		0.23	0.66	F100S0-0.42–0.23	–	3.0	0.6
		0.33	1.18	F100S0-0.42–0.33	–	8.8	1.1

resulting from wall slip, which gives inaccurate measurements of yield stress in water-based suspensions (Saak et al., 2001). The vane measurement system was fitted with a Peltier cooling system for maintaining a constant temperature of 27 deg C.

3.1. Constant shear and hysteresis loop test protocols

Different measurement protocols were applied to the alkali-silicate activated binder pastes to evaluate the transient constant strain rate, the rate dependent, and the thixotropic behaviors. In the constant shear rate tests, the transient response up to the development of steady flow is measured at a constant applied strain rate; a constant angular velocity of 0.1 rad/s was prescribed and the transient shear stress was measured. The rate-dependent shear response was measured over a range of applied shear rates in a hysteresis test. In the hysteresis test, a linear ramp rate of 0.33 s^{-2} was applied up to a strain rate of 40 s^{-1} and then down to 0 s^{-1}. The shear rate sensitivity and deviation from the Newtonian behavior were determined from the measured response [35]. The plastic viscosity (μ) was determined by fitting the Bingham model (equation(1)), to the measured shear response between shear rates (du/dy) equal to 10 and 30 s^{-1} in the down ramp of the hysteresis test response.

$$\tau = \tau_o + \mu\left(\frac{du}{dy}\right)$$

3.2. Equilibrium test protocol (1)

In the equilibrium test, a three-step procedure was followed. Initially, the shear rate was increased from 0 to 200 s^{-1} in the 60s. The shear rate was then held constant at 200 s^{-1} until the shear stress attained a constant value. In the equilibrium test, the continuous decrease in the shear stress at the constant shear rate is due to the breakdown of the flocculates in the suspensions. The attainment of constant shear stress indicates a dynamic steady state at the applied strain rate. The time required for attaining the constant shear stress varied with the paste. After equilibrium, a constant ramp rate of 3 s^{-1} was applied to decrease the shear rate to zero within 60 s. The response with decreasing strain rate is the equilibrium line. The structural buildup in the suspensions following shearing was evaluated from the hysteresis test response on pastes after different rest periods following an equilibrium test. The structure buildup within the suspension is obtained from the hysteretic test after different rest periods, ranging between 0 and 10 min. A new sample was used for evaluating the shearing behavior of a paste after different rest periods.

4. Experimental results

Typical flow curves from the constant shear rate tests on the F90S10 and F50S50 fly ash and slag blends series are shown in Fig. 2. Results from AAFS pastes *sol/b* ratios equal to 0.385 and 0.42 are shown. With increased duration of applied strain, the transient behavior exhibits an increase in stress, which reaches maximum stress. Following the maximum stress, the stress attains a constant value at a large strain. The response immediately following the peak stress, however, varies with the silica content.

At low silica contents in the activating solution, the transient behavior exhibits a classical yield-type behavior with a sharp peak and a decrease in the shear stress following the maximum stress. The peak stress in the constant strain response is identified as the yield stress. With increasing shear strain, a steady-state is attained at constant shear stress, which is lower than the yield stress. In the Maxwell-flow behavior, the transient shear stress gradually attains constant shear stress immediately following the peak stress. The maximum stress in the Maxwell-flow behavior produces steady viscous flow and is identified as the apparent yield stress. With increasing silica content in the activating solution, the transient response changes from a yield-type to a Maxwell-flow behavior. Increasing the silica content in the activating solution initially produces a decrease in the peak stress. On further increasing the silica content the peak stress increases. The lowest peak point in the transient response coincides with the transition from the yield-type to a Maxwell-flow behavior. Nominally similar behavior was obtained from the fly ash pastes (F100S0) and the other fly ash-slag blends with

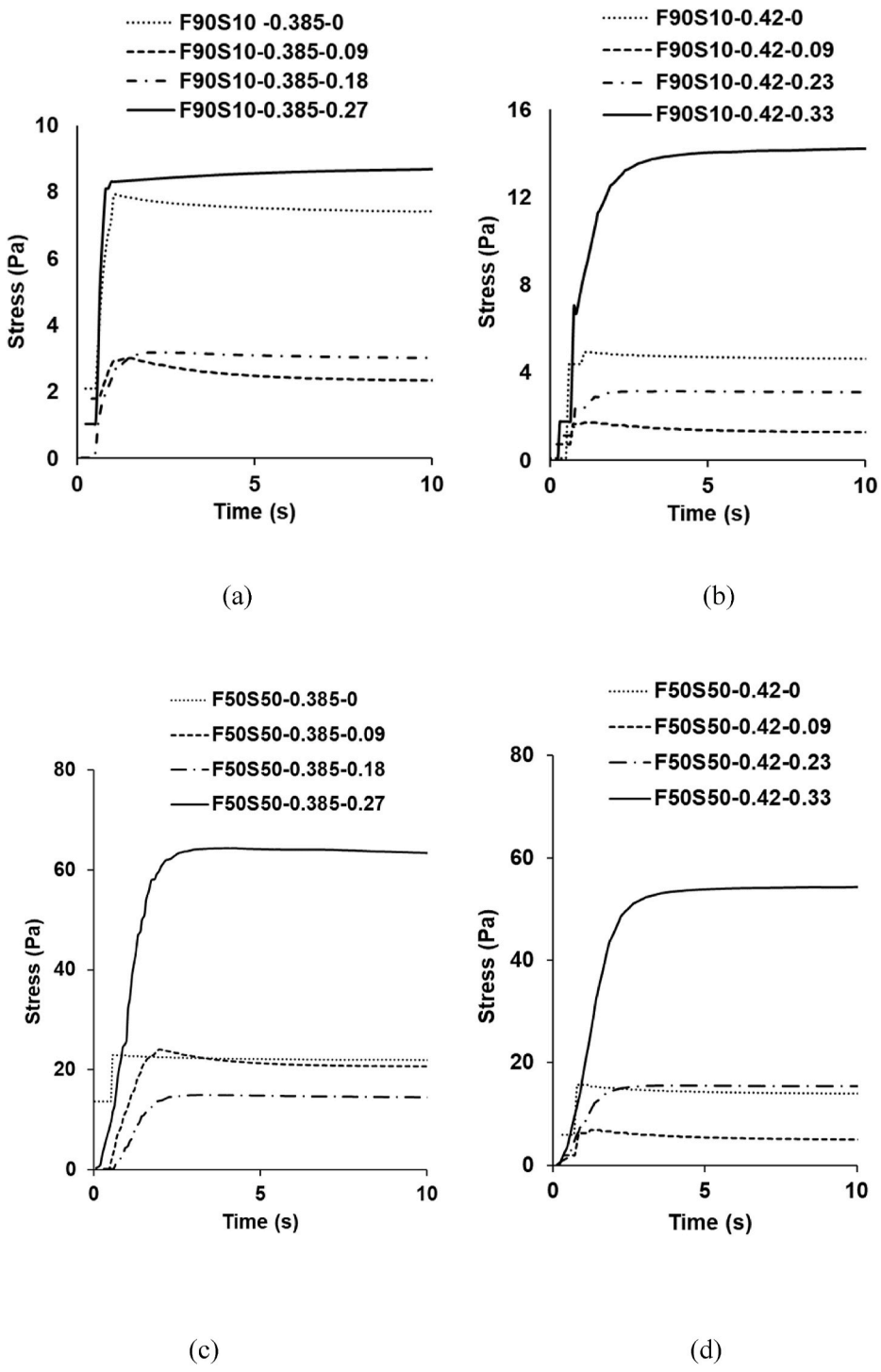

Fig. 2. Constant strain rate response from fly ash/slag blends with different silica contents: (a) F90S10 blends, sol/b = 0.385; (b) F90S10 blends, sol/b = 0.42; (a) F50S50 blends, sol/b = 0.385; (b) F50S50 blends, sol/b = 0.42.

increasing silica content in the activating solution.

The numerical values of the yield stress and the apparent yield stress measured from the different pastes are listed in Table 2. The available data indicates that the observed variation in the transition to flow behavior on increasing the applied shear strain depends on the activating solution composition for all blend proportions and solids loading (*sol/b*) in the paste. For the identical *sol/b*, and fly ash/slag proportions, the maximum stress attained depends on the silica content in the solution.

4.1. Hysteresis test and plastic viscosity

Typical flow curves from the constant shear rate tests on the F90S10 blends with a *sol/b* = 0.385 and F50S50 blends with a *sol/b* = 0.42 are shown in Fig. 3. Only data from pastes covering the ranges of slag contents in the blend and the solids loading are shown for illustrating typical responses. The responses at the low shear rates are shown in the insets for clarity. In mixtures with lower silica contents, the distinct change in slope during the transition from the lower to higher rates indicate change in material behavior. Following the observable change

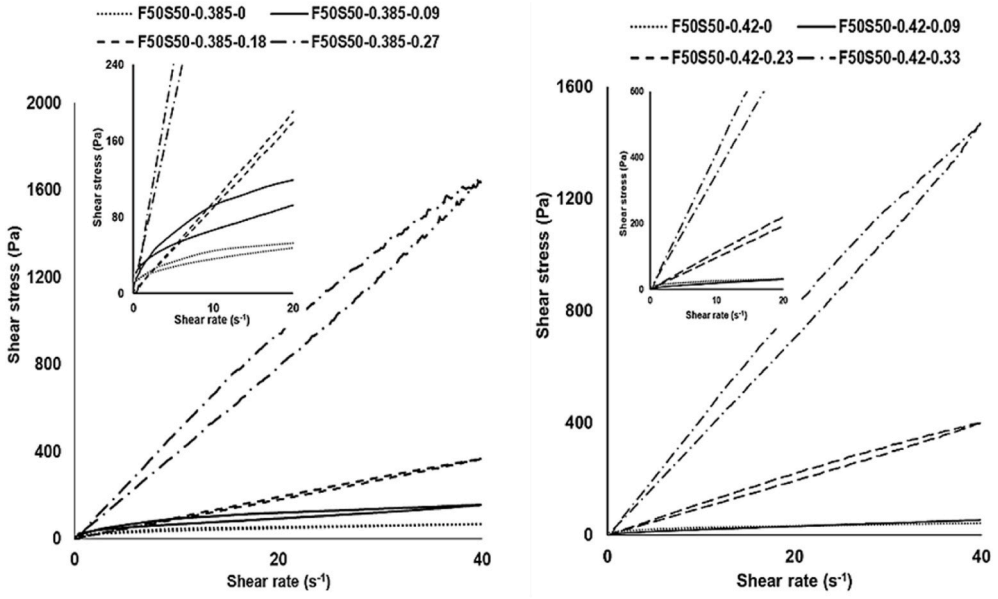

(a) (b)

Fig. 3. Responses measured in Hysteresis test from F50S50 blend with different silica contents: (a) sol/b = 0.385; and (b) sol/b = 0.42.

in slope, there is a progressive shear thinning response. In pastes with higher silica contents, there is a steep increase in the shear stress at lower shear rates indicating the higher resistance of flow due to the highly viscous nature. However, the shear stress with increasing shear rate exhibits a continuous change in slope without the distinctive change in the slope of the shear stress. A shear-thinning response was obtained with an increasing shear rate from all the mixtures tested. The stress as a function of the shear rate depends on the activating solution composition and the slag content in the blend. Significantly higher stress is measured in blends with a higher slag content. At a given slag content, there is an increase in the shear stress at a higher silica content. The slope of the shear stress as a function of shear rate is indicative of the viscosity of the paste. The values of the plastic viscosity for all the pastes evaluated in the test program are listed in Table 2. There is an increase in the viscosity of the AAFS paste with the slag content in the blend and the silica content in the activating solution.

Shearing of a particulate suspension with an internal structure from an at-rest structure results in a large relative movement between the particles and a disruption of the percolated solid network. Flow is produced when the internal structure is disrupted to produce a suspension of particle flocs with predominantly short-range forces between particles. Interaction between the solids phases in the suspension and the fluid medium produces shearing of particle flocs which results in a changing floc structure (Bender and Wagner, 1995). The particle migration can be brought down to minimal in parallel plate tests by adjusting the normal forces (Dai et al., 2013). Up to shear rates of 100 s^{-1}, the contribution of Brownian effects is usually negligible (Bender and Wagner, 1995). As the peclet number increases, the boundary layer becomes thinner, in which the effects of lubrication layer led to shear thickening effect (Foss and Brady, 2000).

In particle suspensions made with $Na_2O.xSiO_2$, which is more viscous than water, the high shear stress on the particle flocs, and the very high shear rates produced in the flow of the activating solution between the particle flocs are responsible for the shear-thinning effect (Kondepudi and Subramaniam 2019). The non-hydrodynamic forces in the shearing fluid creates non-symmetric stress field (Zarraga et al., 2000). The shear flow causes a transition in the viscosity, which is dependent on the volume fraction of solids (Lin et al., 2015). The blends with a higher fly ash content exhibit an insignificant shear-thinning due to the relative ease with which the spherical fly ash particles rearrange under flow induced shear stress. The shear-thinning behavior is more significant for a higher slag content in the blend.

4.2. *Influence of solution composition on yield stress and viscosity*

The variations in maximum stress from the constant shear rate test and the plastic viscosity from the hysteresis tests for the different series are plotted against the silica content in the activating solution in Figs. 4 and 5. Data is plotted for the different blend compositions (the F50S50, F70S30, and the F90S10 series) at different solids loading (*sol/b* ratios equal to 0.385 and 0.42). The M_S of the activating solution is also shown in the graph for reference. The maximum stress identified with yield stress or apparent yield stress, depending on the observed constant shear response are plotted in Figs. 4 and 5 (a). The plastic viscosity obtained from the shear rate response in a hysteresis test is plotted in Figs. 4 and 5 (b). The results indicate that on increasing the silica content, initially there is a decrease in the yield stress. With a further increase in the silica content, a Maxwell flow response is obtained. There is a transition zone observed in which the stress values are decreased or constant for certain silica content before complete transformation to Maxwell response. The yield, transition and Maxwell zones identified, were shown in different line styles in Figs. 4 and 5. The increase in the dissolved silica in the activating solution produces a decrease in the yield stress or an increase in the apparent yield stress. In the Maxwell flow domain, the apparent yield stress increases rapidly with the silica content (and M_S). For a given *sol/b* ratio, higher yield and apparent yield stress values are obtained from blends with higher slag contents. The increase in the apparent yield stress is very sensitive to the silica content at higher slag content.

The addition of silica in the activating solution produces a continuous increase in the plastic viscosity of the fly ash/slag pastes. For a given *sol/b* ratio, AAFS pastes with a higher slag content have a higher viscosity. For instance, the mixture with F50S50 with 0.385 solid loading, exhibited exponential increase in viscosity magnitude from 1.0 to 40.2 Pa s with increase in the silica content. Whereas the mixture with

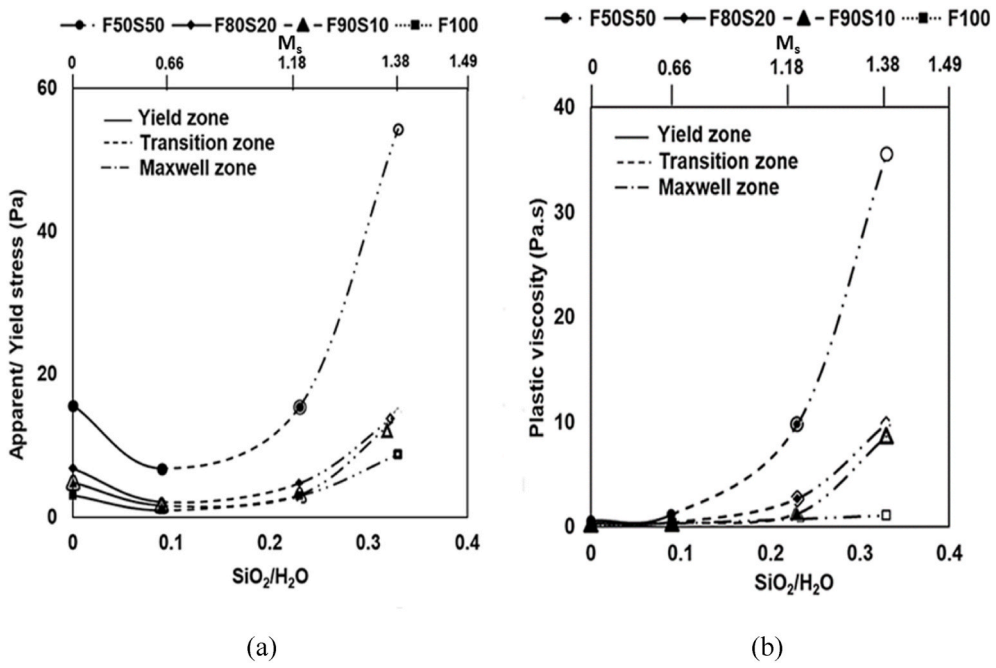

Fig. 4. (a) Variation in the yield stress with silica content for different blends at a sol/b = 0.42; and (b) Variation in the viscosity with silica content for different blends at a sol/b = 0.42.

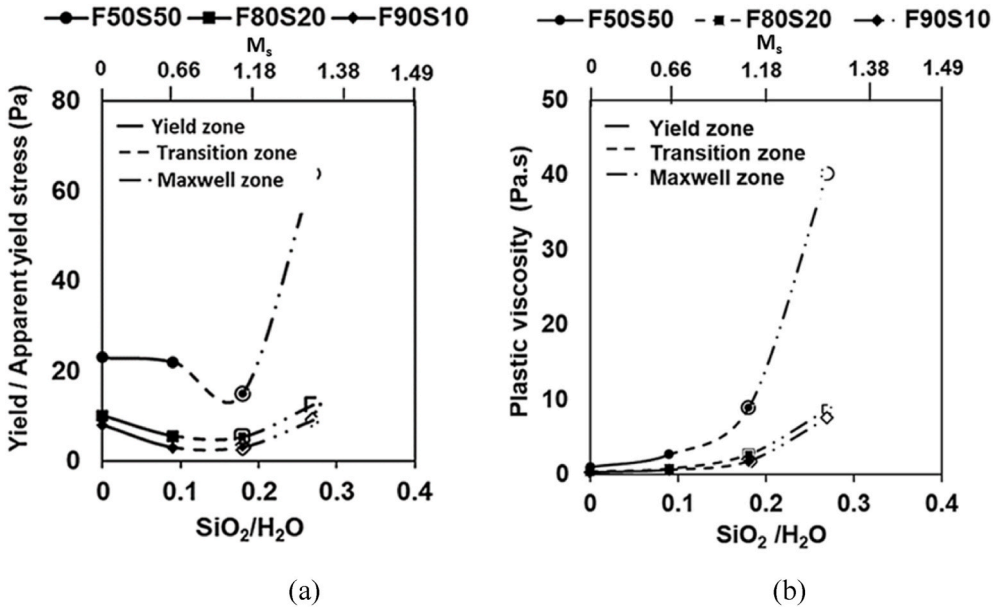

Fig. 5. (a) Variation of yield/apparent yield stress with silica content for different blends and sol/b = 0.385; (b) Variation of the plastic viscosity with silica content for different blends and sol/b = 0.385.

F90S10 with 0.385 solid loading, exhibited an increase in the viscosity of 0.3 Pa s to 7.5 Pa s for a comparable increase in the silica content. The plastic viscosity is very sensitive to the silica content in the Maxwell range; there is a large increase in viscosity with the silica content in pastes, which exhibit a Maxwell flow response. There is a larger increase in the viscosity with silica content in the pastes exhibiting Maxwell flow behavior at higher slag content in the blend.

The transient flow behavior at a constant strain rate varies between yield-type and Maxwell-flow responses, depending on the silica content in the activating solution. In particulate suspensions, yield-type behavior is produced by a percolated particle network capable of resisting applied shear stress (Subramaniam and Wang, 2010). Flow in such suspensions with increasing shear strain produces a large relative motion between the particles (Kim et al., 2016). The ultrasonic measurements were carried out to understand the changes in the early age properties (Wang and Subramaniam, 2011). The Maxwell flow behavior represents a continuous transition into a steady flow with increasing strain, which is typical of a fluid-dominated behavior (Gadkar and Subramaniam 2019).

The change in the composition of the activating solution by the addition of silica, therefore, has the effect of reducing the particle network and leading to a fluid-dominated response. The Maxwell domain is a region where fluid behavior is dominant and an increase in the viscosity of the activating solution between the solid particles

produces a large increase in the plastic viscosity and the apparent yield stress in the constant strain rate response. This fluid domination is produced by increasing the colloidal silica content, which makes the activating solution more viscous (Yang et al., 2008).

4.3. Influence of solids loading on yield stress and plastic viscosity

Yield stress and plastic viscosity for different sol/b ratios in the pastes exhibiting a yield-type behavior are shown in Fig. 6 (a) and (b). Yield stress and plastic viscosity are very sensitive to the increase in the solids loading; there is a very rapid decrease in the yield stress with increasing the *sol/b* ratio. The yield stress also increased with an increase in the replacement percentage of slag in the blend. Solids loading is the most sensitive variable which influences both yield stress and viscosity. Variations in the observed response depend on the compositions of the activating solution and the blend composition. The decrease in the plastic viscosity and yield stress of blends with the addition of fly ash has previously been reported (Yang et al., 2018). For a given fly ash content in the blend, changes in the yield stress and viscosity are produced by the activating solution. With increasing silica content in the activating solution, there is a decrease in the yield stress, while the plastic viscosity increases. The suspension containing no dissolved silica content, which was activated using only sodium hydroxide, was found to have the highest yield stress and lowest viscosity.

4.4. Equilibrium tests and structural buildup

The shear stress response obtained from equilibrium tests on alkali-activated blends for the F90S10 series is plotted in Fig. 7. Data from *sol/b* = 0.385 is plotted in Fig. 5a and b, and responses obtained from pastes with two different silica contents which lie in the yield and Maxwell zones are plotted in Fig. 5a and b. The shear stress measured at a constant shear rate of 200 s^{-1} for obtaining the equilibrium behavior is shown in the inset. The time required to attain the equilibrium shear stress varied between the suspensions. The shearing time required to achieve constant viscosity was 219 s, and 223 s for the F90S10-0.385–0.09, and F90S10-0.385-0.27 suspensions, respectively.

Under constant applied strain rate, the continuous decrease in the viscosity under shearing is indicative of a breakdown of the flocculated structures within the suspension. Under shearing at a constant strain rate, a state of dynamic equilibrium at the lowest energy state of the flocculates structures is attained when the stress reaches a constant value. In the state of dynamic equilibrium, the lowest energy state is attained at the stress level, and the rates of flocculation and structural breakdown are balanced. The data indicates a significantly higher breakdown with silica content. A hysteresis loop is formed between the ramp-up curve and the ramp down curve after the material attains an equilibrium state under shearing at a constant strain rate. After the ramp down following the equilibrium test, the material is in a reference state, which can be used to evaluate the structure build up. The shear response obtained from the decreasing shear rate response, is therefore the equilibrium line connecting the reference and the equilibrium states.

The structural build up in the AAFS pastes was evaluated from the shear response obtained after different rest periods following the equilibrium test. The shear stress response obtained at 0, 5, and 10 min after the equilibrium test is shown in Fig. 8. The F90S10-0.385–0.09 and F90S10-0.385–0.27 correspond to pastes that exhibit the yield-type and Maxwell flow response, respectively. The low shear rate response is shown in the inset for clarity. In the paste with the lower silica content, which exhibited a yield-type behavior, there is a recovery of yield stress evident in the low shear rate response. There is a very rapid yield stress recovery within 5 min and it increases beyond the initial yield stress. There is also a very rapid increase in the shear stress at any shear rate with time in this paste. In the suspension with the higher silica content, the lack of yield stress is evident in the low strain response, which exhibits a nearly linear increase with strain rate. In this paste, there is a very small change in the response to increasing strain rate with rest time.

Changes in the shearing response (up ramp of the hysteresis test) relative to the equilibrium line after a defined rest period are indicative of changes in the flocculated state of the suspended particles in the at-rest state within the suspension. In the pastes exhibiting yield-type behavior, the changes are associated with the rebuilding of the flocculated structure with time. In pastes exhibiting Maxwell-flow behavior, the response after increasing rest periods indicates very small changes in the viscous response with shear rates. The internal build up of a long-range particle structure inside the suspension is obtained from the yield stress behavior at the low strain rates. Changes in the state of flocculation after defined rest periods were evaluated by calculating the area between the stress response to increasing strain rate (up ramp) and the equilibrium line. The specific rebuilding energy is obtained as the area under the measured flow response after the yield for shear rates between 50 and 150 s^{-1}. The SRE is related to the changes in the flocculated structure within the suspension (Kim et al., 2016). The hysteresis loop tests help in quantifying the thixotropic rebuilding (Ferron

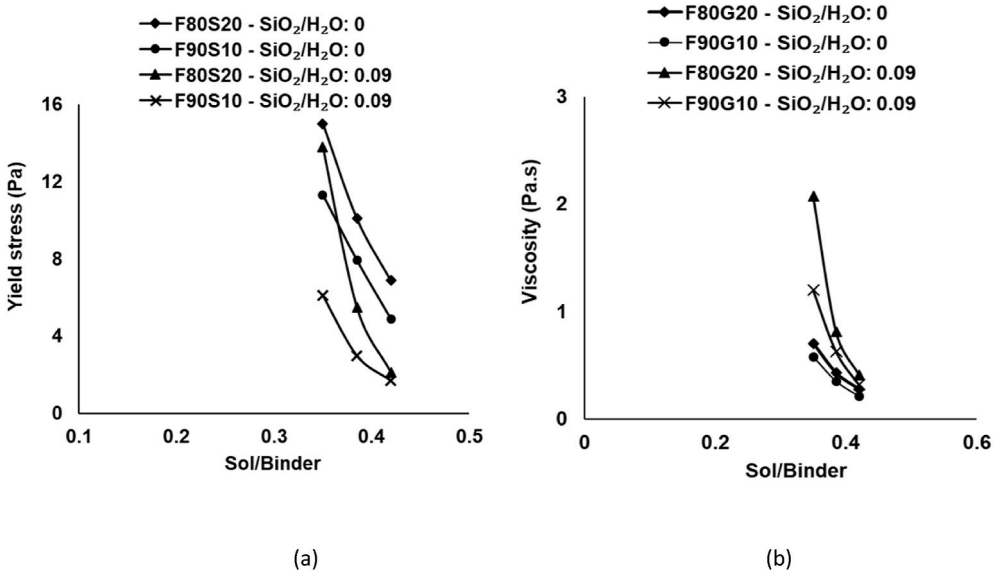

Fig. 6. (a) Yield stress as a function of sol/b ratio; and (b) Plastic viscosity as a function of sol/b ratio.

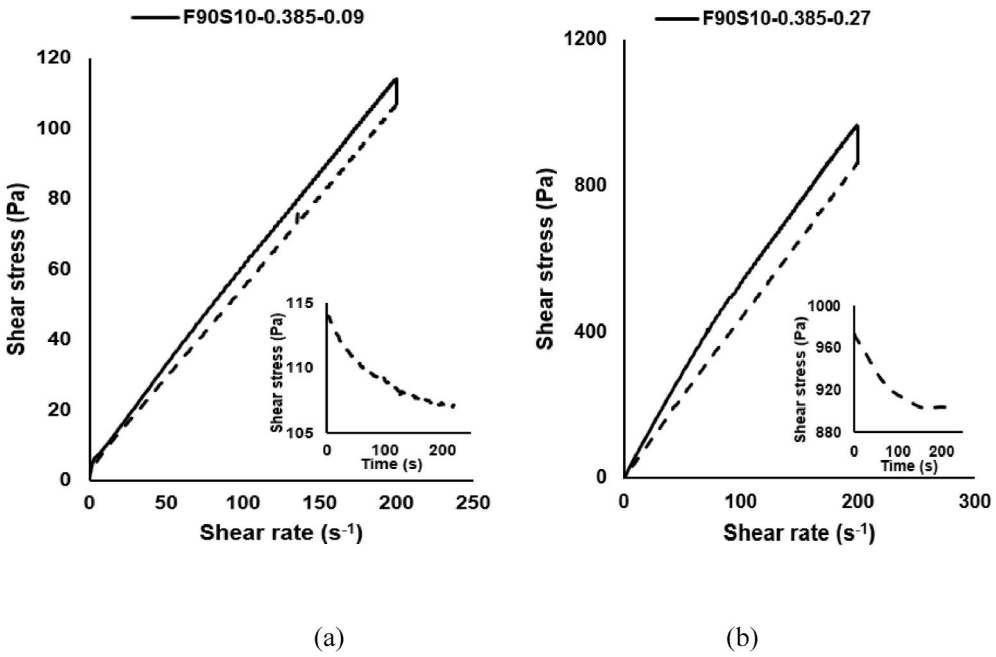

Fig. 7. Equilibrium curves for F90S10 blends for sol/b = 0.385 (a) for silica content of 0.09; (b) for silica content of 0.27.

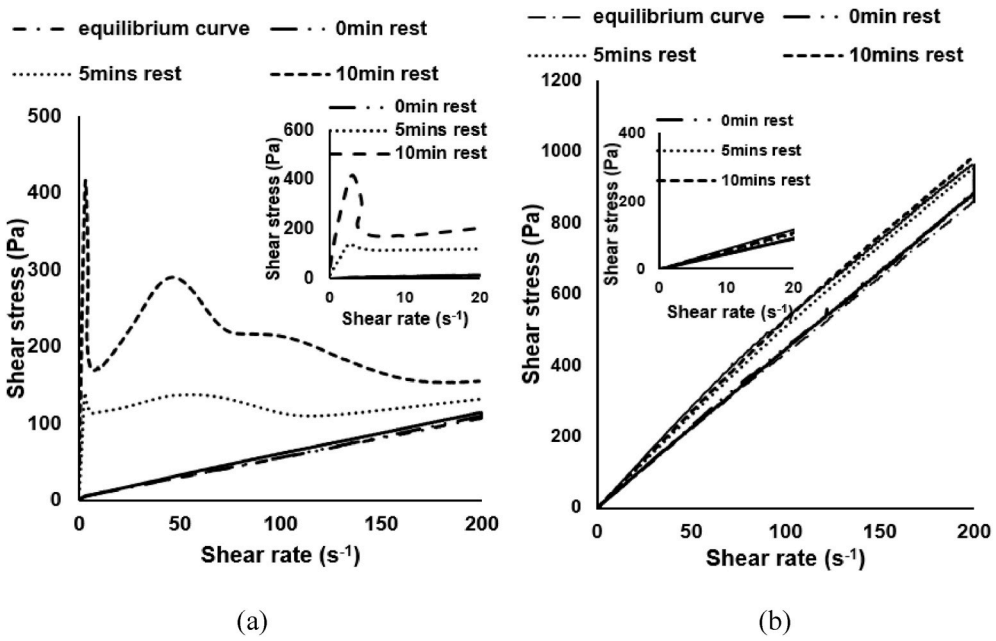

Fig. 8. Hysteresis tests showing structural recovery after different rest periods: (a) for F90S10 blends for sol/b ratio of 0.385 and silica content of 0.09; and (b) for F90S10 fly-ash and slag blends for sol/b ratio of 0.385 and silica content of 0.27.

et al., 2007). The procedure for determining SRE is presented in detail in (Kondepudi, K., and Samarakoon et al., 2019). The equilibrium area, which is the area under the equilibrium line between shear rates of 50 and 150$s^{-1,}$ was also computed. The SRE was normalized with the equilibrium area and is plotted in Fig. 9 for the alkali-activated blends with F90S10-0.385–0.09 and F90S10-0.385–0.27. The structural rebuilding energy (SRE) is very rapid in suspensions with lower silica content in the activating solution. There is a more rapid increase in the normalized SRE in pastes with yield-type behavior when compared with the pastes which exhibit Maxwell flow response. The available data indicates that in pastes, which exhibit a yield-type behavior, the increase in SRE with age is higher in pastes with a higher slag content. While the addition of silica produces a decrease in the yield stress, there is an increase in SRE with age on the addition of silica in the pastes with yield stress. This corresponds with the loss of the workability of the paste.

5. Discussion

The observed flow behavior is influenced by the solution composition, the solids loading, and the slag present in the system. The composition of the activating solution has the effect of producing variations in the transient flow behavior at a constant shear rate. The variations in the values of yield/apparent yield and viscosity depend on the solids loading and the slag content in the blend. The composition of the

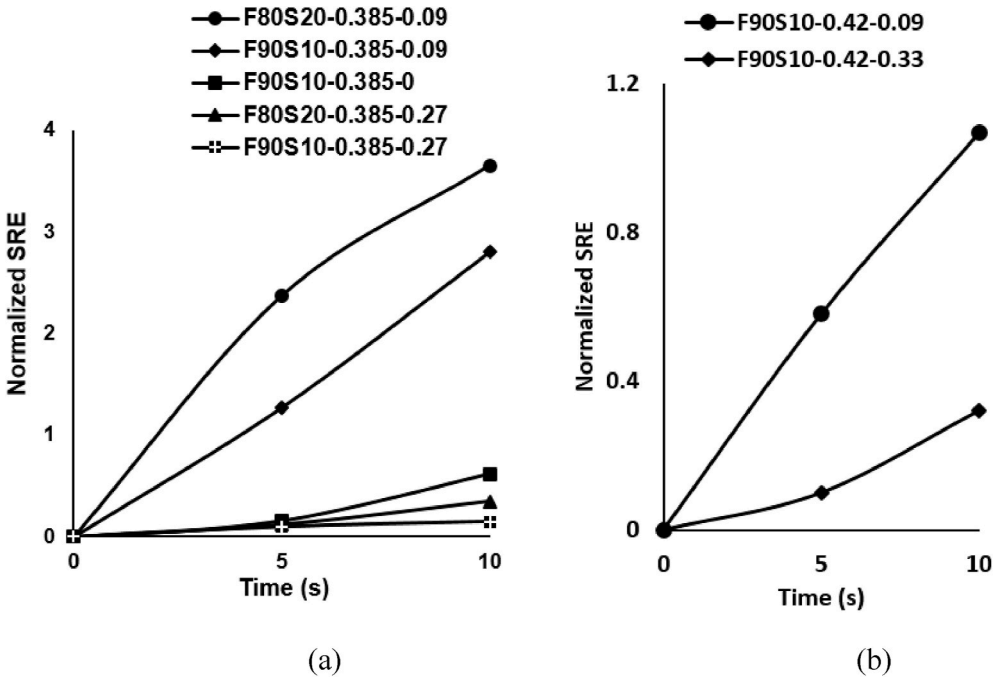

Fig. 9. Normalized structural rebuilding energy for different rest periods after equilibrium for different *sol/b* ratios: (a) 0.385; and (b) 0.42.

activating solution is defined by the silica content and the M_S. The composition of the activating solution influences its viscosity and also the dispersed state of particles in the suspension. The zeta potential of the fly ash and slag particles are influenced by the pH of the solution. With the increase in molarity of NaOH, there is an increase in the zeta potential, which favors the aggregation of particles increasing the yield stress (Kondepudi and Subramaniam, 2019). The available data indicate that the zeta potential of slag becomes more negative with pH (Mercado-Borrayo et al., 2013). For the given molarity of NaOH, increasing the silica content in the sodium silicate solution makes the zeta potential of fly ash particles in suspension more negative, which has the effect of decreasing the yield stress (Kondepudi and Subramaniam, 2019). Additions of lower dosages of sodium silicate in the slag system, increases the magnitude of the zeta potential halving the yield stress of the paste. This is due to increase in repulsive forces because of double layer formation. The silicate anions get adsorbed on the surface of slag which carry the positive charges (Ca^{2+}, Na^{+}). Additions of silicate decreases the yield stress in the fly ash and slag blends due its plasticizing and de-flocculating effect of silicate anions (Kondepudi, K., and Subramaniam, 2019). The particle-particle interactions are influenced by the activator nature (Kashani et al., 2014). The presence of dissolved silica in the solution also promotes the precipitation of calcium silicate hydrates due to the Ca^{2+} released from slag dissolution. Increasing the sodium silicate leads to an increased formation of gel, by producing additional calcium silicate hydrate in the system, which contributes to an increase in the yield stress. The counteracting influences of the zeta potential and gel formation contribute to the observed variation in yield stress with sodium silicate content.

An increase in the activating solution viscosity produces higher yield stress in the particulate suspension. The viscosity of the $Na_2O.xSiO_2$ solution depends on the silica content and the M_S. For a constant silica content, the viscosity of the sodium silicate solution decreases with an increase in M_S and reaches a minimum at an M_S of 1.80 (Yang et al., 2008). Since the molarity of the NaOH was kept fixed, increasing the silica content in the activating solution produced an increase in the M_S. With increasing silica content in the alkali-silica solution, there are two counteracting effects of an increase in viscosity with silica content and a decrease produced by an increase in M_S. For low silica content, the influence of M_S in decreasing the viscosity of the activating solution is more dominant than the increasing effect of added silica. At higher silica content, the influence of added silica on increasing the viscosity is more dominant than the influence of M_S in decreasing the viscosity.

The influence of silica addition on the viscosity of the activating solution is to produce a decrease or negligible increase in the viscosity at low silica contents and a significant increase in the viscosity at higher silica contents. At low silica contents, the combined effect of negligible change in the solution viscosity and a decrease in the potential to agglomerate, leads to a decrease in the yield stress with silica content. Increasing the silica content further produces a fluid-dominated response of the increasingly viscous activating solution and the decreasing tendency of the particles to agglomerate. This produces the transition to the Maxwell-flow response from a yield-type behavior. The Maxwell-flow response is therefore produced in pastes, where the fluid response dominates the transient behavior under increasing strain. The increase in the plastic viscosity of the paste is directly linked with the activating solution viscosity. In the pastes, which exhibit a yield-type behavior, increasing silica content produces a negligible increase in the viscosity. The fluid-dominated Maxwell-type response, however, exhibits a higher sensitivity to the increase in the silica content in the activating solution.

The solids content and the blend composition produce variations in the transient response and influence the individual values of yield stress and viscosity. For a given activating solution composition, increasing the solids content produce pastes with higher yield stress and viscosity. Increasing the solids content in a particulate suspension has the influence of decreasing the inter-particle distances leading to increasing dominance of the short-range van der Waals forces of attraction (Wallevik 2005). The theoretical estimate of rheological properties was reported to be valid if the coarse particles are spherical in geometry (Chateau et al., 2008). This results in a very rapid increase in the yield stress with the *sol/b* ratio. The increase in the viscosity is related to the particulate effect in particulate suspension (Lin et al., 2015).

The composition of the blend, the relative proportions of fly ash, and slag also influence the viscosity and yield stress of the pastes. Overall, fly ash influences rheology by reducing both viscosity and yield stress. The spherical nature of the fly ash particles allows relative motion, hence

producing decreases in the resistance to initiate flow (in both yield and Maxwell regions) and during flow with increasing shear strain (Barnes 1997). The addition of slag produces an increase in yield without significantly increasing the viscosity at low silica contents. At high silica content, in the Maxwell zone, there are rapid increases in both the yield stress and viscosity with silica content. The slag particles are angular and contribute to increased resistance to the initiation of flow and steady flow under constant shear strains.

An increase in the slag content in the blend impacts the thixotropic behavior of the blends. The addition of slag accelerates the increase in yield stress in low silica systems after shearing. Further, the setting behavior indicated by the increase in SRE is accelerated. The SRE is found to be influenced by the yield and Maxwell domains. Both chemical aging and reversible flocculation contribute to the observed thixotropic behavior (Feys et al., 2007). Shearing produces a finely dispersed suspension of particles. The reversible structure formation is significantly faster to develop in pastes that exhibit yield-type behavior due to the higher potential for agglomeration. The increase in the yield stress with age above the initial values before shearing is produced by the aging effect resulting in reaction products forming at the points of contact (Roussel et al., 2012). The rapid structural build-up takes place with the suspensions containing silica content that falls in the yield domain. In pastes that exhibit Maxwell flow, after shearing, the reassembly of an internal percolated network of particles produced by the electrostatic and van der Waals forces is slow to develop. The aging effect is therefore significantly enhanced by slag content in the blend. The addition of slag contributes to the enhanced production of chemical linkages due to enhanced reaction in the presence of dissolved silica in the solution (Reddy et al., 2020). However, it was reported that the AAS is more prone to water loss when compared to Portland cement and AAF (Thomas et al., 2017). The increased MgO in the slag may lead to formation of hydrotalcite which causes 9% volume increase in the hydrates (Winnefeld et al., 2015). The chemical aging from the increase in the chemical linkages produces an irreversible loss of workability. The SRE is higher in suspensions with higher percentages of slag due to the precipitation of calcium silicate hydrates, which accelerates the setting process, thereby increasing its yield compared to viscosity.

Controlling rheology for specific applications requires regulating the viscosity, yield stress, and thixotropy. Rheology control can be achieved by varying the activating solution composition, the slag content in the blend, and the sol/b ratio. Pastes with solid dominant behavior, which exhibit yield stress and those with liquid dominant Maxwell-flow response, show dramatic differences in the yield stress, structural recovery, and viscosity. For self-levelling and pumping applications, compositions with low viscosity and low yield-type behavior, are preferable. The suspensions exhibiting Maxwell type behavior has apparent yield stress and high viscosity which is not a suitable option for pumping and extrusion process in construction applications. The rheology control for lowering the yield stress within the yield-type binders can be obtained from the added silica in the activating solution. The higher dosages of silica content in the activating solution give higher stress to increasing shear strain, which is however from a fluid-dominated behavior. In applications where shape retention is required, such as layer deposition or printing, this division helps in selecting the composition of the solution suitable for printing. The compositions which exhibit a Maxwell flow response with an apparent yield behavior would be unfavorable for printing applications.

The alkali-activated blends with high yield stress recovery and less viscosity in the yield dominant zone create high possible conditions for 3D concrete printing. High yield is achieved for low silica content and low sol/b ratio. For a given sol/b ratio, the yield can be increased without significantly increasing the viscosity by increasing the slag dosage. Within the yield zone, at low silica contents, the yield stress can be decreased by silica addition. The addition of silica in the yield zone provides for a faster thixotropic buildup. This yield dominant and structural recovery behavior is highly favorable for printing conditions. This increase in static yield stress property enables shape retention property. The composition of pastes is often determined by the requirements of silica content and NaOH molarity for strength and other performance requirements. The rheology control in such cases would require additional additives (Kondepudi and Subramaniam, 2021b). The fluid dominant behavior is induced in the absence of CMC in fly ash/slag binary blends which is unfavorable for the 3D printing construction process (Kondepudi and Subramaniam, 2020).

6. Conclusions

The rheological characterization of alkali-activated fly-ash and slag blends was carried out on different solid loadings with different solution compositions. The rheological characterization of blends replacing fly-ash with slag by 10%–50% was performed to understand the effect of slag on flow behavior. The alkali-activated blend suspensions were prepared with alkali solutions varying with a silica modulus of the solution below 1.67 and fixed alkalinity of solution from NaOH. The solutions were prepared with constant molarity of 3 M with varying modulus by altering the colloidal sodium silicate in the solution to understand the effect of the solution M_S on the rheological behavior of suspensions. From rheological investigation, the following conclusions are drawn.

1. At low silica content in the activating solution (low values of M_S), a yield-type behavior is obtained from the pastes. While the yield stress decreases, the plastic viscosity of the paste increases with the silica content in the activating solution. Increasing the slag content in the blend produces an increase in the yield stress. The influence of slag content on the paste viscosity is minimal.
2. With increasing silica content, the transient shear response under constant applied shear rate transitions to a fluid-dominated Maxwell-flow response with apparent yield stress. In the Maxwell flow region, increasing the silica content in the activating solution content results in large increases in plastic viscosity and apparent yield stress of the paste.
3. Both yield stress and plastic viscosity of the paste increase with an increase in the solids loading.
4. The thixotropic response differs in pastes that exhibit yield-type and Maxwell-flow behaviors. The structural re-building is rapid in the solid dominant zone (yield zone) whereas, in the fluid dominant zone (Maxwell zone) the buildup of structure is slow. Structural re-building energy increases with the increase in the percentage of slag replacement with fly-ash. Structural recovery is faster at higher solid loading.
5. Comparing the sodium hydroxide activated suspensions with alkali-silica activated suspensions, the yield stress recovery and structural rebuilding energy increase are rapid with additional dissolved silica within the solid dominated yield zone. The addition of silica enhances the structural buildup in the solid-dominated region leading to a rapid increase in yield stress with time.

Data availability

Some or all data, models, or code that support the findings of this study are available from the corresponding author upon reasonable request.

Declaration of competing interest

The authors declare that they have no known competing financial interests or personal relationships that could have appeared to influence the work reported in this paper.

Acknowledgments

The authors would like to acknowledge support from the Department of Science and Technology, Initiative to Promote Energy Efficient Habitant (I-PHEE) Grant No. TMD/CERI/BEE/2016/031.

References

Albitar, M., Mohamed Ali, M.S., Visintin, P., Drechsler, M., 2017. Durability evaluation of geopolymer and conventional concretes. Construct. Build. Mater. 136 (1), 374–385. https://doi.org/10.1016/j.conbuildmat.2017.01.056.

Alghamdi, H., Nair, S.A., Neithalath, N., 2019. Insights into material design, extrusion rheology, and properties of 3D-printable alkali-activated fly ash-based binders. Mater. Des. 167, 107634. https://doi.org/10.1016/j.matdes.2019.107634.

Arbi, K., Nedeljkovic, M., Zuo, Y., Ye, G., 2016. A review on the durability of alkali-activated fly ash/slag systems: advances, issues, and perspectives. Ind. Eng. Chem. Res. 55 (19), 5439–5453. https://doi.org/10.1021/acs.iecr.6b00559.

Barnes, H.A., 1997. Thixotropy—a review. J. Non-Newtonian Fluid Mech. 70 (1–2), 1–33. https://doi.org/10.1016/S0377-0257(97)00004-9.

Bender, J.W., Wagner, N.J., 1995. Optical measurement of the contributions of colloidal forces to the rheology of concentrated suspensions. J. Colloid Interface Sci. 172 (1), 171–184.

Benito, P., Leonelli, C., Medri, V., Vaccari, A., 2013. Geopolymers: a new and smart way for sustainable development. Appl. Clay Sci. 73, 1. https://doi.org/10.1016/j.clay.2013.03.008.

Bernal, S.A., Provis, J.L., 2014. Durability of alkali-activated materials: progress and perspectives. J. Am. Ceram. Soc. 97 (4), 997–1008. https://doi.org/10.1111/jace.12831.

Bhagath Singh, G.V., Subramaniam, K.V., 2017. Evaluation of sodium content and sodium hydroxide molarity on compressive strength of alkali activated low-calcium fly ash. Cement andConcrete Composites 81, 122–132. https://doi.org/10.1016/j.cemconcomp.2017.05.001.

Bhagath Singh, G.V.P., Subrahmanyam, C., Subramaniam, K.V.L., 2018. Dissolution of the glassy phase in low-calcium fly ash during alkaline activation. Adv. Cement Res. 30 (7), 313–322. https://doi.org/10.1680/jadcr.17.00170.

Bhagath Singh, G.V.P., Subramaniam, K.V.L., 2019a. Influence of processing temperature on the reaction product and strength gain in alkali-activated fly ash. Cement Concr. Compos. 95, 10–18. https://doi.org/10.1016/j.cemconcomp.2018.10.010.

Bhagath Singh, G.V.P., Subramaniam, K.V., 2019b. Effect of active components on strength development in alkali-activated low calcium fly ash cements. Journal of Sustainable Cement-Based Materials 8 (1), 1–19. https://doi.org/10.1080/21650373.2018.1520657.

Bhagath Singh, G.V.P., Subramaniam, K.V., 2020. Evaluation of total reactive oxide ratios and working solution ratios on strength development in fly ash–based geopolymers. J. Mater. Civ. Eng. 32 (4), 04020051 https://doi.org/10.1061/(ASCE)MT.1943-5533.0003109.

Chang, J.J., 2003. A study on the setting characteristics of sodium silicate-activated slag pastes. Cement Concr. Res. 33 (7), 1005–1011. https://doi.org/10.1016/S0008-8846(02)01096-7.

Chateau, X., Ovarlez, G., Trung, K.L., 2008. Homogenization approach to the behavior of suspensions of noncolloidal particles in yield stress fluids. J. Rheol. 52 (2), 489–506. https://doi.org/10.1122/1.2838254.

Chithiraputhiran, S., Neithalath, N., 2013. Isothermal reaction kinetics and temperature dependence of alkali activation of slag, fly ash and their blends. Construct. Build. Mater. 45 https://doi.org/10.1016/j.conbuildmat.2013.03.061, 233-2.

Dai, S.C., Bertevas, E., Qi, F., Tanner, R.I., 2013. Viscometric functions for noncolloidal sphere suspensions with Newtonian matrices. J. Rheol. 57 (2), 493–510. https://doi.org/10.1122/1.4774325.

Duxson, P., Fernández-Jiménez, A., Provis, J.L., Lukey, G.C., Palomo, A., van Deventer, J. S., 2007. Geopolymer technology: the current state of the art. J. Mater. Sci. 42 (9), 2917–2933. https://doi.org/10.1007/s10853-006-0637-z.

Fang, G., Ho, W.K., Tu, W., Zhang, M., 2018. Workability and mechanical properties of alkali-activated fly ash-slag concrete cured at ambient temperature. Construct. Build. Mater. 172, 476–487. https://doi.org/10.1016/j.conbuildmat.2018.04.008.

Ferron, R.P., Gregori, A., Sun, Z., Shah, S.P., 2007. Rheological method to evaluate structural buildup in self-consolidating concrete cement pastes. ACI Mater. J. 104 (3), 242.

Fernández-Jiménez, A., Puertas, F., 2001. Setting of alkali-activated slag cement. Influence of activator nature. Adv. Cement Res. 13 (3), 115–121. https://doi.org/10.1680/adcr.13.3.115.39288.

Feys, D., Verhoeven, R., De Schutter, G., 2007. Evaluation of time independent rheological models applicable to fresh self-compacting concrete. Appl. Rheol. 17 (5), 56244–57190. https://doi.org/10.1515/arh-2007-0018.

Foss, D.R., Brady, J.F., 2000. Structure, diffusion and rheology of Brownian suspensions by Stokesian dynamics simulation. J. Fluid Mech. 407, 167–200. https://doi.org/10.1017/S0022112099007557.

Fu, Y., Cai, L., Yonggen, W., 2011. Freeze–thaw cycle test and damage mechanics models of alkali-activated slag concrete. Construct. Build. Mater. 25 (7), 3144–3148. https://doi.org/10.1016/j.conbuildmat.2010.12.006.

Gadkar, A., Subramaniam, K.V.L., 2019. An evaluation of yield and Maxwell fluid behaviors of fly ash suspensions in alkali-silicate solutions. Mater. Struct. 52 (6), 117. https://doi.org/10.1617/s11527-019-1429-7.

Gao, X., Yu, Q.L., Brouwers, H.J.H., 2015. Characterization of alkali activated slag–fly ash blends containing nano-silica. Construct. Build. Mater. 98, 397–406. https://doi.org/10.1016/j.conbuildmat.2015.08.086.

Kashani, A., Provis, J.L., Qiao, G.G., van Deventer, J.S., 2014. The interrelationship between surface chemistry and rheology in alkali activated slag paste. Construct. Build. Mater. 65, 583–591. https://doi.org/10.1016/j.conbuildmat.2014.04.127.

Kim, J.H., Yim, H.J., Ferron, R.D., 2016. In situ measurement of the rheological properties and agglomeration on cementitious pastes. J. Rheol. 60 (4), 695–704. https://doi.org/10.1122/1.4954251.

Kondepudi, K., Subramaniam, K.V., 2019. Rheological characterization of low-calcium fly ash suspensions in alkaline silicate colloidal solutions for Geopolymer concrete production. J. Clean. Prod. 234, 690–701. https://doi.org/10.1016/j.jclepro.2019.06.124.

Kondepudi, K., Subramaniam, K.V., 2020. Advances in Rheology and AM Extrusion Based 3D Printing Performance of Alkali-Activated Binders. ACI, ID.M-2020-424.R2.

Kondepudi, K., Subramaniam, K.V., 2021a. Critical evaluation of rheological behavior of low-calcium fly ash geopolymer pastes. Adv. Cement Res. 1–11. https://doi.org/10.1680/jadcr.20.00043.

Kondepudi, K., Subramaniam, K.V., 2021b. Formulation of alkali-activated fly ash-slag binders for 3D concrete printing. Cement Concr. Compos. 119 https://doi.org/10.1016/j.cemconcomp.2021.103983.

Lavergne, F., Belhadi, R., Carriat, J., Fraj, A.B., 2019. Effect of nano-silica particles on the hydration, the rheology and the strength development of a blended cement paste. Cement Concr. Compos. 95, 42–55.

Lee, N.K., Lee, H.K., 2015. Reactivity and reaction products of alkali-activated, fly ash/slag paste. Construct. Build. Mater. 81, 303–312. https://doi.org/10.1016/j.conbuildmat.2015.02.022.

Lee, N.K., Lee, H.K., 2013. Setting and mechanical properties of alkali-activated fly ash/slag concrete manufactured at room temperature. Construct. Build. Mater. 47, 1201–1209. https://doi.org/10.1016/j.conbuildmat.2013.05.107.

Lin, Y., Phan-Thien, N., Khoo, B.C., 2015. Shear induced organization of particles in non-colloidal suspensions in steady shear flow. J. Non-Newtonian Fluid Mech. 223, 228–232. https://doi.org/10.1016/j.jnnfm.2015.07.006.

Lootens, D., Hébraud, P., Lécolier, E., Van Damme, H., 2004. Gelation, shear-thinning and shear-thickening in cement slurries. Oil Gas Sci. Technol. 59 (1), 31–40. https://doi.org/10.2516/ogst:2004004.

Makul, N., 2020. Modern sustainable cement and concrete composites: review of current status, challenges and guidelines. Sustainable Materials and Technologies 25, e00155. https://doi.org/10.1016/j.susmat.2020.e00155.

Marjanović, N., Komljenović, M., Baščarević, Z., Nikolić, V., Petrović, R., 2015. Physical–mechanical and microstructural properties of alkali-activated fly ash–blast furnace slag blends. Ceram. Int. 41 (1), 1421–1435. https://doi.org/10.1016/j.ceramint.2014.09.075.

Mercado-Borrayo, B.M., Schouwenaars, R., González-Chávez, J.L., Ramírez-Zamora, R. M., 2013. Multi-analytical assessment of iron and steel slag characteristics to estimate the removal of metalloids from contaminated water. Journal of Environmental Science and Health, Part A 48 (8), 887–895. https://doi.org/10.1080/10934529.2013.761492.

Nath, P., Sarker, P.K., 2014. Effect of GGBFS on setting, workability and early strength properties of fly ash geopolymer concrete cured in ambient condition. Construct. Build. Mater. 66, 163–171. https://doi.org/10.1016/j.conbuildmat.2014.05.080.

Olivas, A., Helsel, M.A., Martys, N.S., Ferraris, C.F., George, W.L., Ferron, R., 2016. Rheological Measurement of Suspensions without Slippage: Experiment and Model. NIST Technical Note 1946. NIST, Gaithersburg, MD. https://doi.org/10.6028/NIST.TN.1946.

Pacheco-Torgal, F., Abdollahnejad, Z., Camões, A.F., Jamshidi, M., Ding, Y., 2012. Durability of alkali-activated binders: a clear advantage over Portland cement or an unproven issue? Construct. Build. Mater. 30, 400–405. https://doi.org/10.1016/j.conbuildmat.2011.12.017.

Palacio, M., Puertas, F., Banfill, P.F.G., 2008. Rheology and setting of alkali-activated slag pastes and mortars: effect of organ admixture. ACI Mater. J. 105 (2), 140–148.

Puertas, F., Varga, C., Alonso, M.M., 2014. Rheology of alkali-activated slag pastes. Effect of the nature and concentration of the activating solution. Cement Concr. Compos. 53, 279–288. https://doi.org/10.1016/j.cemconcomp.2014.07.012.

Puertas, F., González-Fonteboa, B., González-Taboada, I., Alonso, M.M., Torres-Carrasco, M., Rojo, G., Martínez-Abella, F., 2018. Alkali-activated slag concrete: fresh and hardened behaviour. Cement Concr. Compos. 85, 22–31.

Ravikumar, D., Neithalath, N., Peethamparan, S., 2010. Structure and strength of NaOH activated concretes containing fly ash or GGBFS as the sole binder. Cement Concr. Compos. 32 (6), 399–410. https://doi.org/10.1016/j.cemconcomp.2010.03.007.

Reddy, K.C., Gudur, C., Subramaniam, K.V., 2020. Study on the influences of silica and sodium in the alkali-activation of ground granulated blast furnace slag. Construct. Build. Mater. 257, 119514. https://doi.org/10.1016/j.conbuildmat.2020.119514.

Roussel, N., Ovarlez, G., Garrault, S., Brumaud, C., 2012. The origins of thixotropy of fresh cement pastes. Cement Concr. Res. 42 (1), 148–157. https://doi.org/10.1016/j.cemconres.2011.09.004.

Saak, A.W., Jennings, H.M., Shah, S.P., 2001. The influence of wall slip on yield stress and viscoelastic measurements of cement paste. Cement Concr. Res. 31 (2), 205–212. https://doi.org/10.1016/S0008-8846(00)00440-3.

Samarakoon, M.H., Ranjith, P.G., Rathnaweera, T.D., Perera, M.S.A., 2019. Recent advances in alkaline cement binders: a review. J. Clean. Prod. 227, 70–87. https://doi.org/10.1016/j.jclepro.2019.04.103.

Subramaniam, K.V., Wang, X., 2010. An investigation of microstructure evolution in cement paste through setting using ultrasonic and rheological measurements. Cement Concr. Res. 40 (1), 33–44. https://doi.org/10.1016/j.cemconres.2009.09.018.

Thomas, R.J., Lezama, D., Peethamparan, S., 2017. On drying shrinkage in alkali-activated concrete: improving dimensional stability by aging or heat-curing. Cement Concr. Res. 91, 13–23. https://doi.org/10.1016/j.cemconres.2016.10.003.

Vázquez-Quesada, A., Tanner, R.I., Ellero, M., 2016. Shear thinning of noncolloidal suspensions. Phys. Rev. Lett. 117 (10), 108001. https://doi.org/10.1103/PhysRevLett.117.108001.

Wang, X., Subramaniam, K.V.L., 2011. Ultrasonic monitoring of capillary porosity and elastic properties in hydrating cement paste. Cement Concr. Compos. 33 (3), 389–401. https://doi.org/10.1007/978-94-007-0723-8_63.

Wallevik, J.E., 2005. Thixotropic investigation on cement paste: experimental and numerical approach. J. Non-Newtonian Fluid Mech. 132 (1–3), 86–99. https://doi.org/10.1016/j.jnnfm.2005.10.007.

Winnefeld, F., Ben Haha, M., Le Saout, G., Costoya, M., Ko, S.C., Lothenbach, B., 2015. Influence of slag composition on the hydration of alkali-activated slags. Journal of Sustainable Cement-Based Materials 4 (2), 85–100. https://doi.org/10.1080/21650373.2014.955550.

Yang, X., Zhu, W., Yang, Q., 2008. The viscosity properties of sodium silicate solutions. J. Solut. Chem. 37 (1), 73–83. https://doi.org/10.1007/s10953-007-9214-6.

Yang, K.H., Jung, Y.B., Cho, M.S., Tae, S.H., 2015. Effect of supplementary cementitious materials on reduction of CO2 emissions from concrete. J. Clean. Prod. 103, 774–783. https://doi.org/10.1016/j.jclepro.2014.03.018.

Yang, T., Zhu, H., Zhang, Z., Gao, X., Zhang, C., Wu, Q., 2018. Effect of fly ash microsphere on the rheology and microstructure of alkali-activated fly ash/slag pastes. Cement Concr. Res. 109, 198–207.

Yaragal, S.C., Kumar, B.C., Jitin, C., 2020. Durability studies on ferrochrome slag as coarse aggregate in sustainable alkali activated slag/fly ash based concretes. Sustainable Materials and Technologies 23, e00137. https://doi.org/10.1016/j.susmat.2019.e00137.

Ye, H., Radlińska, A., 2016. Fly ash-slag interaction during alkaline activation: influence of activators on phase assemblage and microstructure formation. Construct. Build. Mater. 122, 594–606. https://doi.org/10.1016/j.conbuildmat.2016.06.099.

You, N., Liu, Y., Gu, D., Ozbakkaloglu, T., Pan, J., Zhang, Y., 2020. Rheology, shrinkage and pore structure of alkali-activated slag-fly ash mortar incorporating copper slag as fine aggregate. Construct. Build. Mater. 242, 118029. https://doi.org/10.1016/j.conbuildmat.2020.118029.

Zarraga, I.E., Hill, D.A., Leighton Jr., D.T., 2000. The characterization of the total stress of concentrated suspensions of noncolloidal spheres in Newtonian fluids. J. Rheol. 44 (2) https://doi.org/10.1122/1.551083, 671-671.

Zannerni, G.M., Fattah, K.P., Al-Tamimi, A.K., 2020. Ambient-cured geopolymer concrete with single alkali activator. Sustainable Materials and Technologies 23, e00131. https://doi.org/10.1016/j.susmat.2019.e00131.

Zhuang, X.Y., Chen, L., Komarneni, S., Zhou, C.H., Tong, D.S., Yang, H.M., Wang, H., 2016. Fly ash-based Geopolymer: clean production, properties and applications. J. Clean. Prod. 125, 253–267. https://doi.org/10.1016/j.jclepro.2016.03.019.